Supporting Information for

Catalytic Transitions in the Human MDR1 P-Glycoprotein Drug Binding Sites

John G. Wise

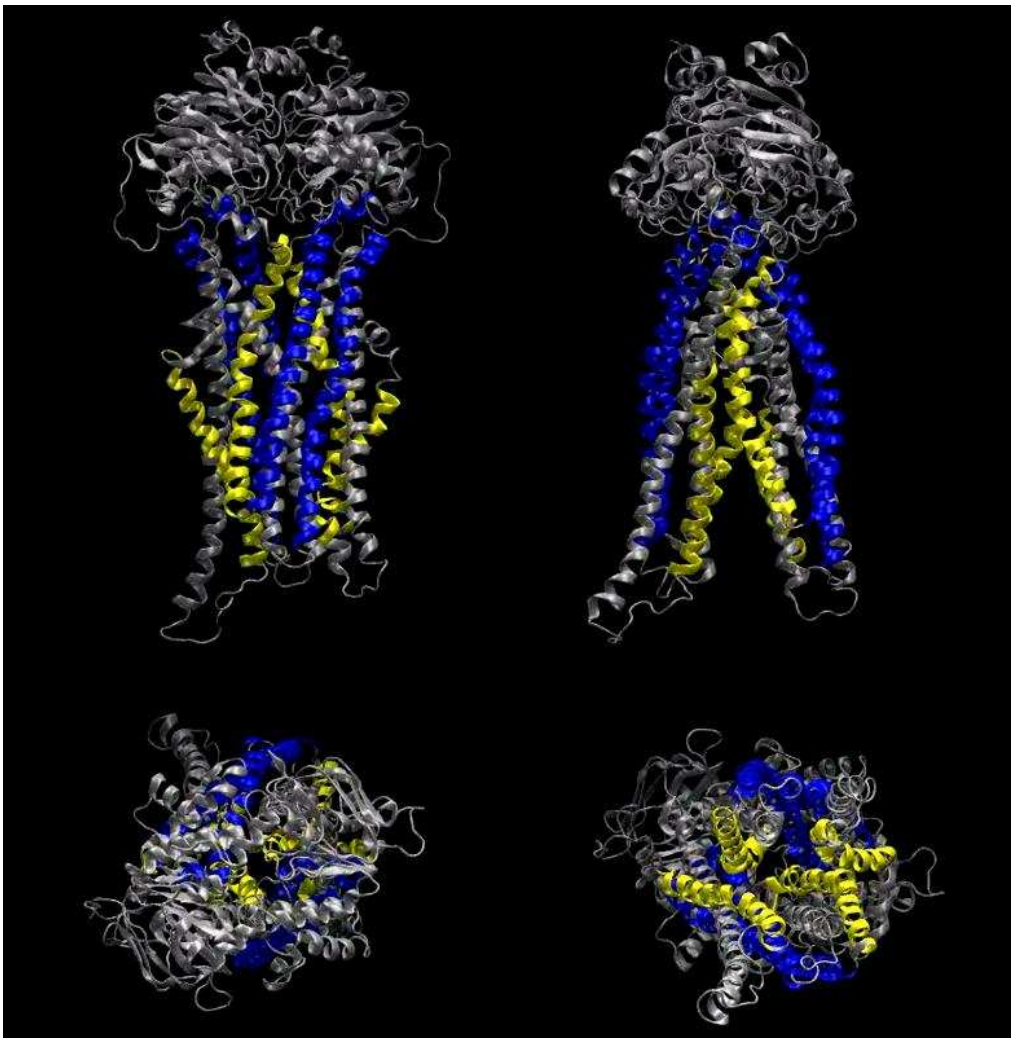

[Hyperlink to video – SupportingVideo1.mpg]

Supporting Figure S1. Video of human P-glycoprotein dynamics. The 26 nonredundant structures identified from the "wide opened to the cytoplasm" to the "wide opened to the extracellular space" targeted molecular dynamics simulations were used to make a video of the dynamics of Pgp. The protein backbone is shown in ribbon representation. Helices 4/10 and 5/11 (blue) show the largest relative movements, while helices 1/3 and 7/9 that make up the putative ligand exit gate are shown in yellow. The top left figure shows a side view of the protein that emphasizes the closing of the nucleotide binding domains. The top right figure shows a side view emphasizing the opening of the drug binding sites (about a 90° rotation relative to the top left image. The bottom left image views Pgp from the cytoplasmic space above the nucleotide binding domains and emphasizes the twisting of the NBDs as closure is achieved. The bottom right figure shows Pgp from the extracellular space looking into the drug binding sites. In this image one can observe the dramatic opening of the drug binding sites to the extracellular space as the ADP-Vi transition state is achieved.

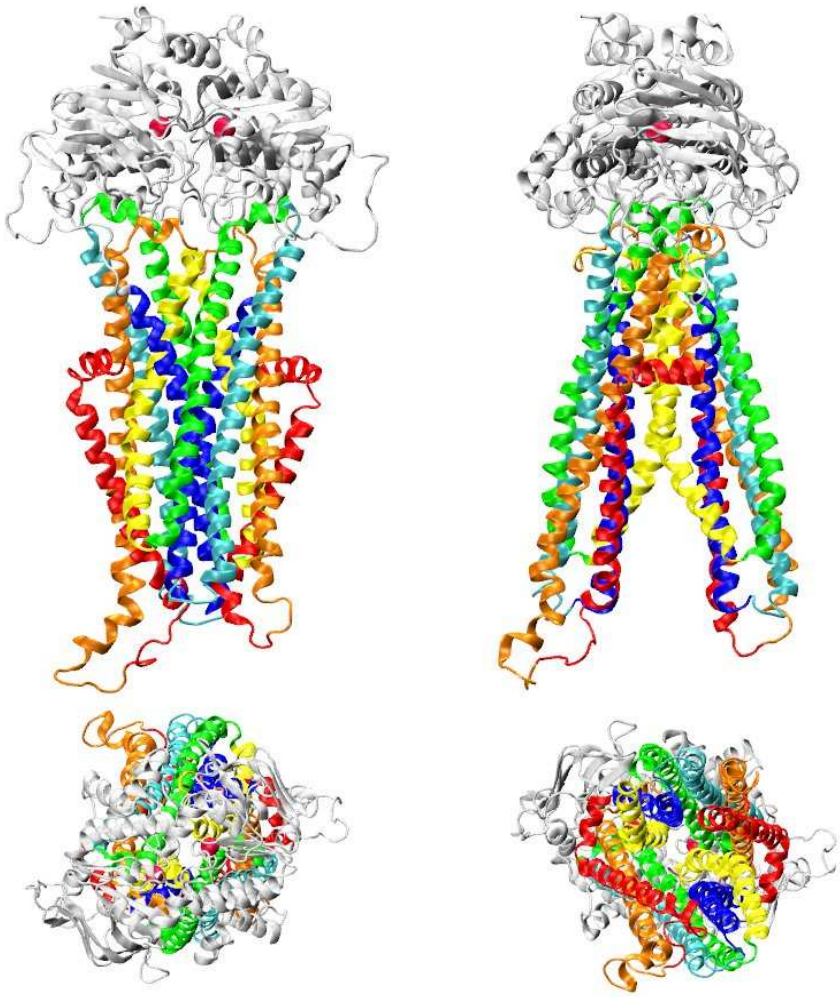

[Hyperlink to video – SupportingVideo2.mpg]

Supporting Figure S2. Video of human P-glycoprotein dynamics including color-coded transmembrane helices. Same as Supporting Video S1 except that transmembrane helices have been color coded as follows. Helices 1/7 red, 2/8 orange, 3/9 yellow, 4/10 green, 5/11 cyan and 6/12 are blue. For reference note that Helix 1 is to the left in the upper left frame, in the foreground in the upper right frame, to the left in the lower left frame and to the left in the lower right-hand frame. Catalytic glutamyl residue Cα atoms in the NBDs are represented with red van der Waals spheres.

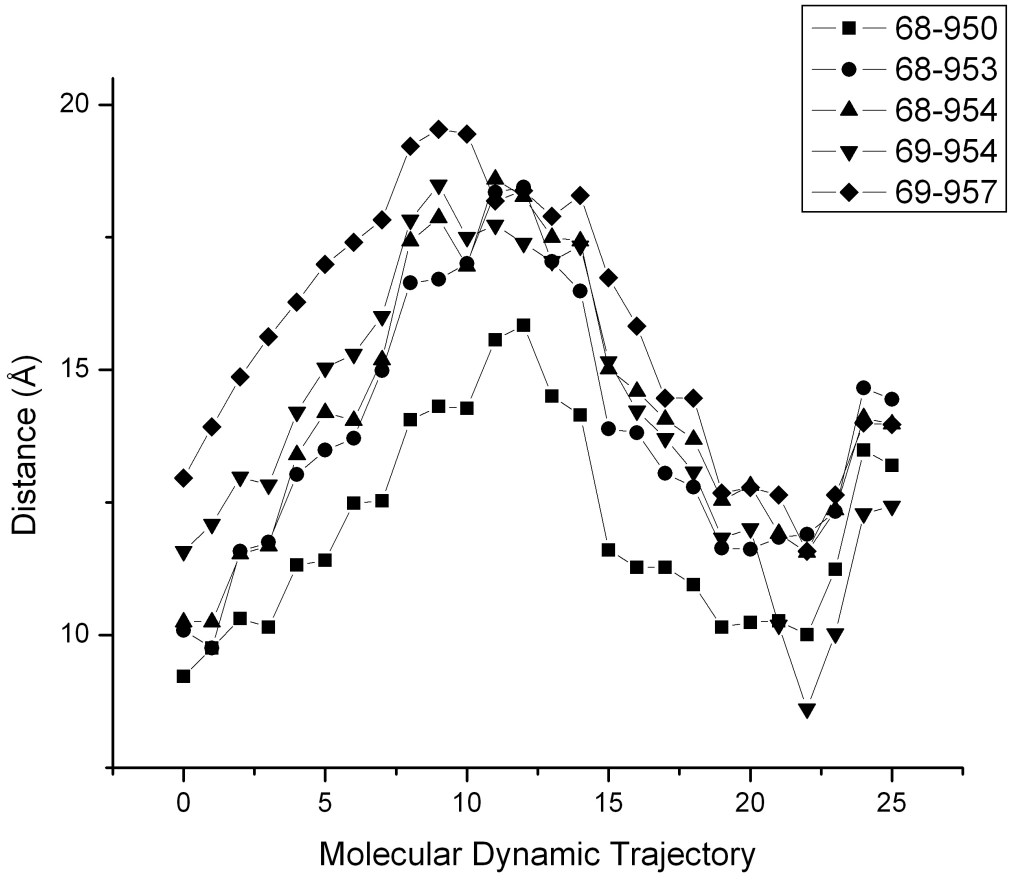

Supporting Figure S3. TM1 and TM11 Relative Helical Movements During Simulated Catalysis. The figure shows the Cα to Cα distances calculated for each of the 26 nonredundant structures as Pgp moved from a "wide open to the inside" to a "wide open to the outside" conformation. The residues analyzed, 68 and 69 of TM 1 and residues 950, 953, 954 and 957 of TM 11, were identified in *(1)* as the only 5 pairs of residues (all on TM1) that were able to be cross-linked to TM 11 out of 350 possible pairs at the external ends of TMs 1, 3, 4, 5 and 6. The cross-links observed in *(1)* only occurred if ATP was hydrolyzed by the transporter.

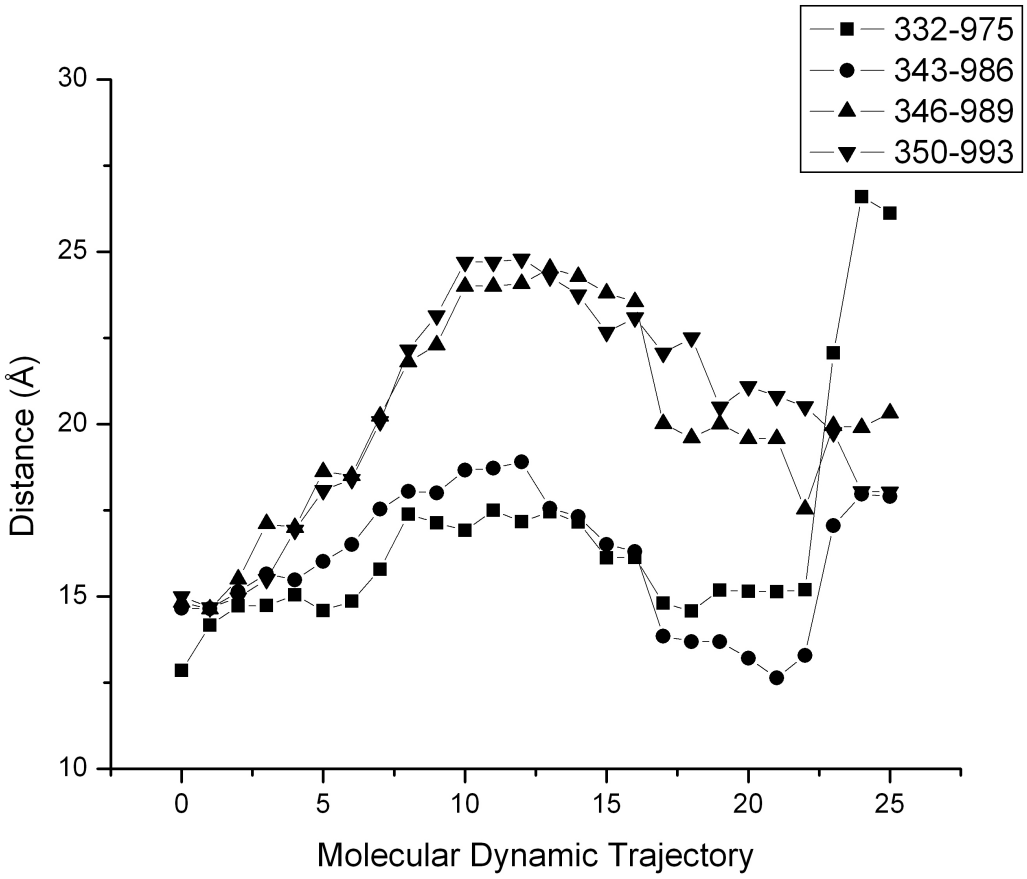

Supporting Figure S4. Residues of TM6 and TM12 that Form Disulfide Bonds during ATP Hydrolysis. Figure S4 shows the Cα to Cα distances calculated for each of the 26 nonredundant structures as Pgp moved from a "wide open to the inside" to a "wide open to the outside" conformation. The residues analyzed were located on TMs 6 and 12 and are indicated in the Figure. These residues formed disulfide bonds only during ATP hydrolysis *(2)*.

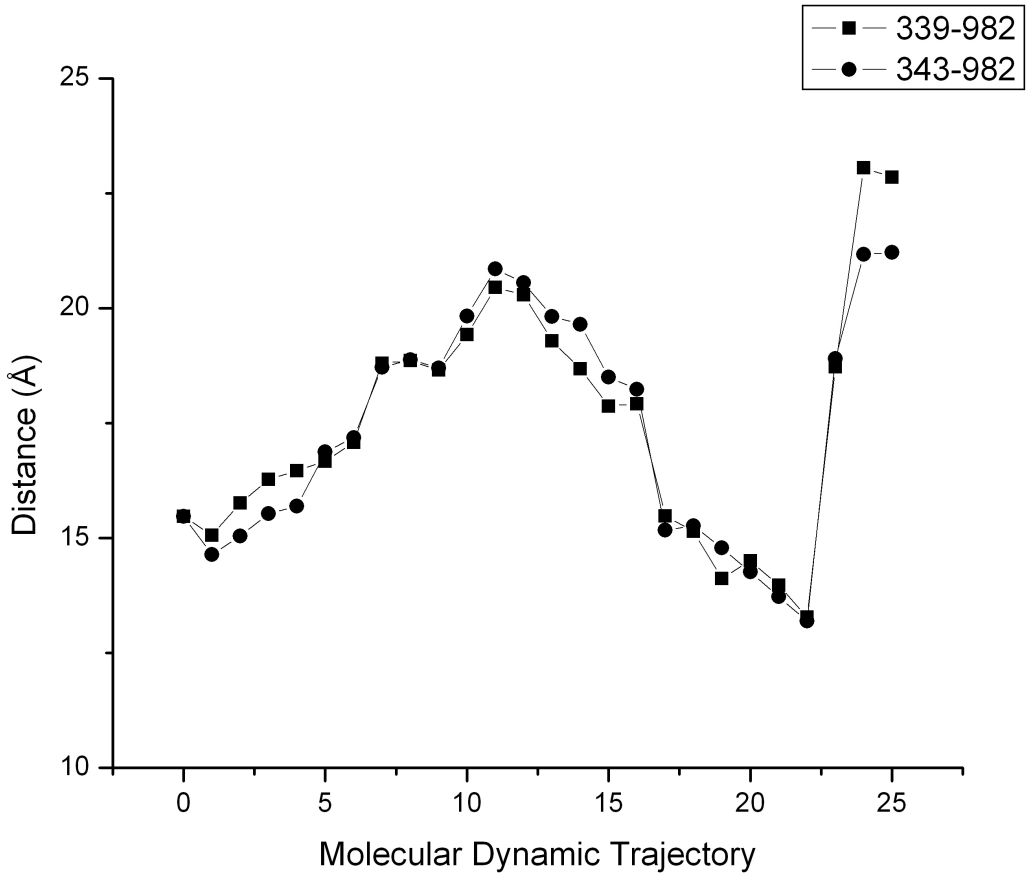

Supporting Figure S5. Residues of TM6 and TM12 that From Crosslinks with a Tris-Maleimide. Figure S5 shows the Cα to Cα distances calculated for each of the 26 nonredundant structures as Pgp moved from a "wide open to the inside" to a "wide open to the outside" conformation. The residues from TMs 6 and 12 are indicated in the Figure. Crosslinking of residues 339-982 with Tris-(2-maleimidoethyl)amine inhibited Pgp ATP hydrolysis while crosslinking of 343-982 was enhanced by ATP hydrolysis *(3)*.

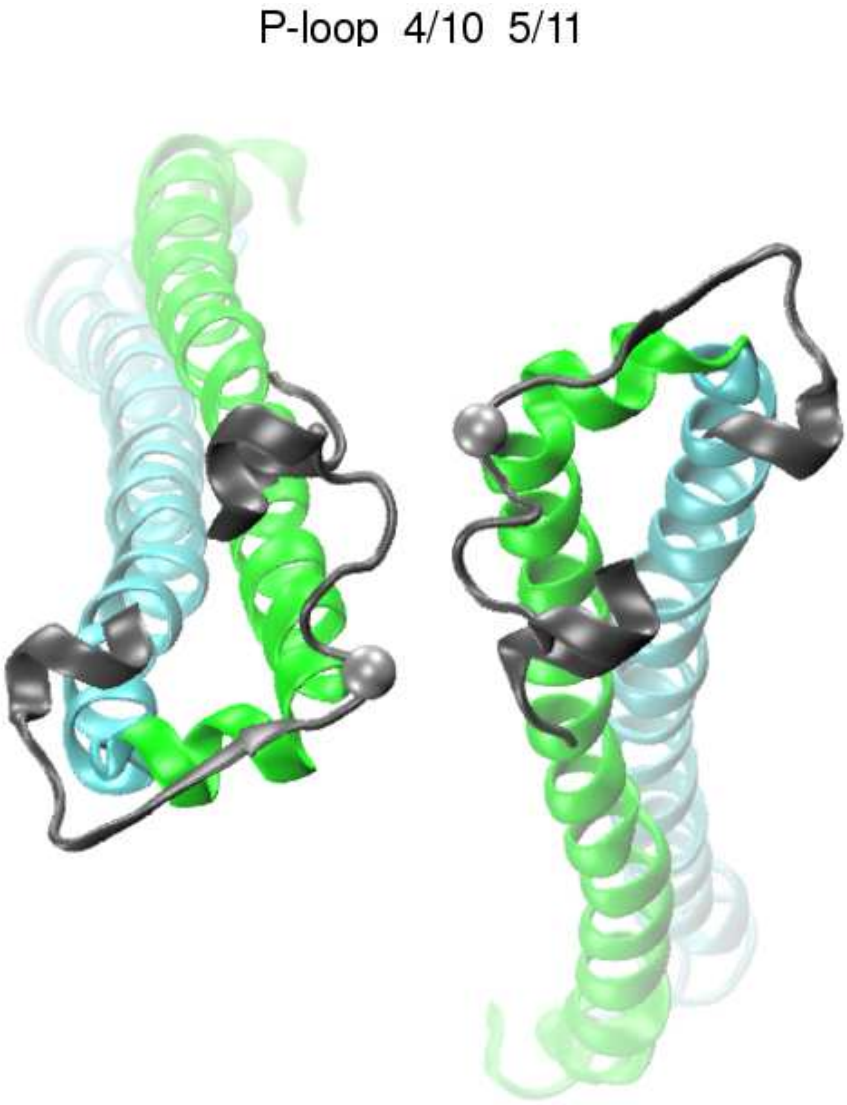

[Hyperlink to video – SupportingVideo3.mpg]

Supporting Figure S6. Helical movements in Pgp as the transition state structure is approached. The video begins with depictions of the P-loop and adjacent structures of the two nucleotide binding domains shown in gray ribbons with the Cα atoms of the two catalytic glutamyl residues shown as van der Waal's spheres. The rest of the nucleotide binding domain

structures were left out of the video so that the drug binding domain conformational changes could be more easily observed. The view of the transporter is from above the nucleotide binding domains looking toward the cytoplasmic face of the membrane. Three frames from the nonredundant Pgp structures corresponding to frames 23-25 (approach to the transition state – see text) are shown repeated 3 times throughout the entire video. In the subsequent video segment, helices 4/10 (green) and 5/11 (cyan) with coupling helices 2 and 4 (short green helices) are added and the sequence is repeated again 3 times. In the third sequence, helices 6 /12 (blue) are added. Subsequent video sequences add helices 3/9 (yellow), 2/8 (orange) and 1/7 (red) to the composite protein structure. The coordinated movements of nucleotide binding domains, coupling helices and drug binding domain helices 4/5, 10/11, as well as the connected movements of helices 3/9 and 6/12 to open the external face of the drug binding domain to the extracellular space are discussed in the text. The structures shown in each video segment are listed at the top of the video. Helices are colored in order of the visual spectrum with helices 1/7 in red and helices 6/12 in dark blue.

The video shows the slight twist of coupling helix 2 (left side of Figure S2) relative to coupling helix 4 (right side of the video) which is presumably driven by nucleotide binding domain conformational changes as bound ATP approaches its hydrolytic transition state. The associated straightening of helices 4/5 and 10/11 and the consequent coupled movement of helices 3/9 (connected via very short externally located loops with 4/10) and helices 6/12 (which are connected to the 5/11 helices by short externally located loops) moves the external face of the drug binding domain in a coordinated manner to its fully opened to the outside transition state conformation. Less movement of helices 1/7 and 2/8 during this transition is apparent, consistent

with the more quantitative data of Figure 3 which shows most of the dramatic opening of the drug binding domain to the outside occurring with helices 4/10, 5/11, 3/9 and 6/12.

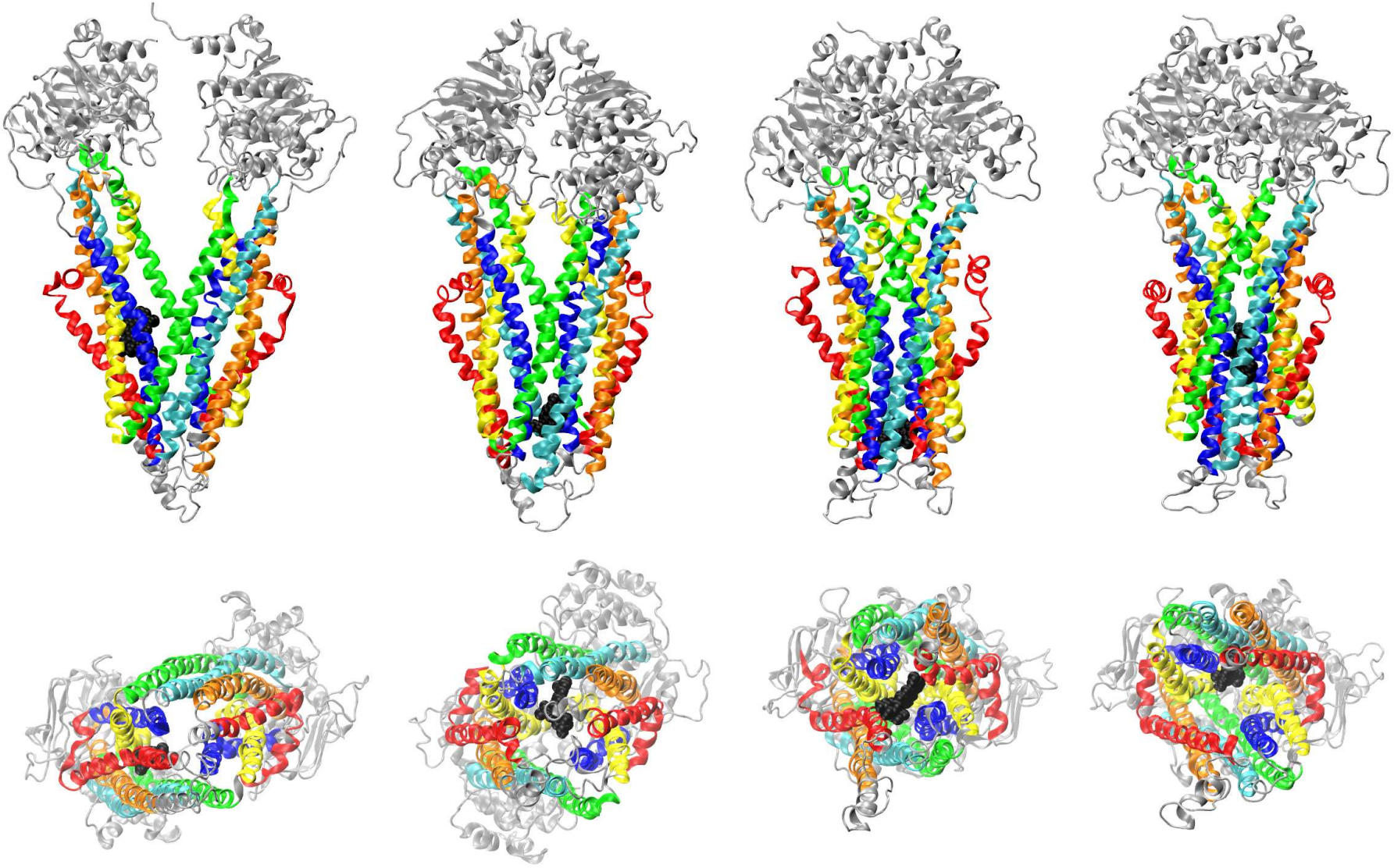

Supporting Figure S7. Docking interactions of daunorubicin with the drug binding domain of Pgp with color-coded DBD helices. The protein backbone is shown in cartoon representation with the transmembrane helices shown with the following color code: Helices 1/7 red, 2/8 orange, 3/9 yellow, 4/10 green, 5/11 cyan and 6/12 are blue. For reference note that Helix 1 (red) is to the left in all frames and helices 4 and 5 (green and cyan) are positioned in the foreground of all upper frames and oriented to the top of all lower frames. Daunorubicin is shown in space-filling representations in black. Pgp and daunorubicin are shown in the fully open inward, partially opened inward, partially opened outward and fully opened outward conformations (left to right, respectively) in side views (top row) and in a view from the extracellular space (bottom row).

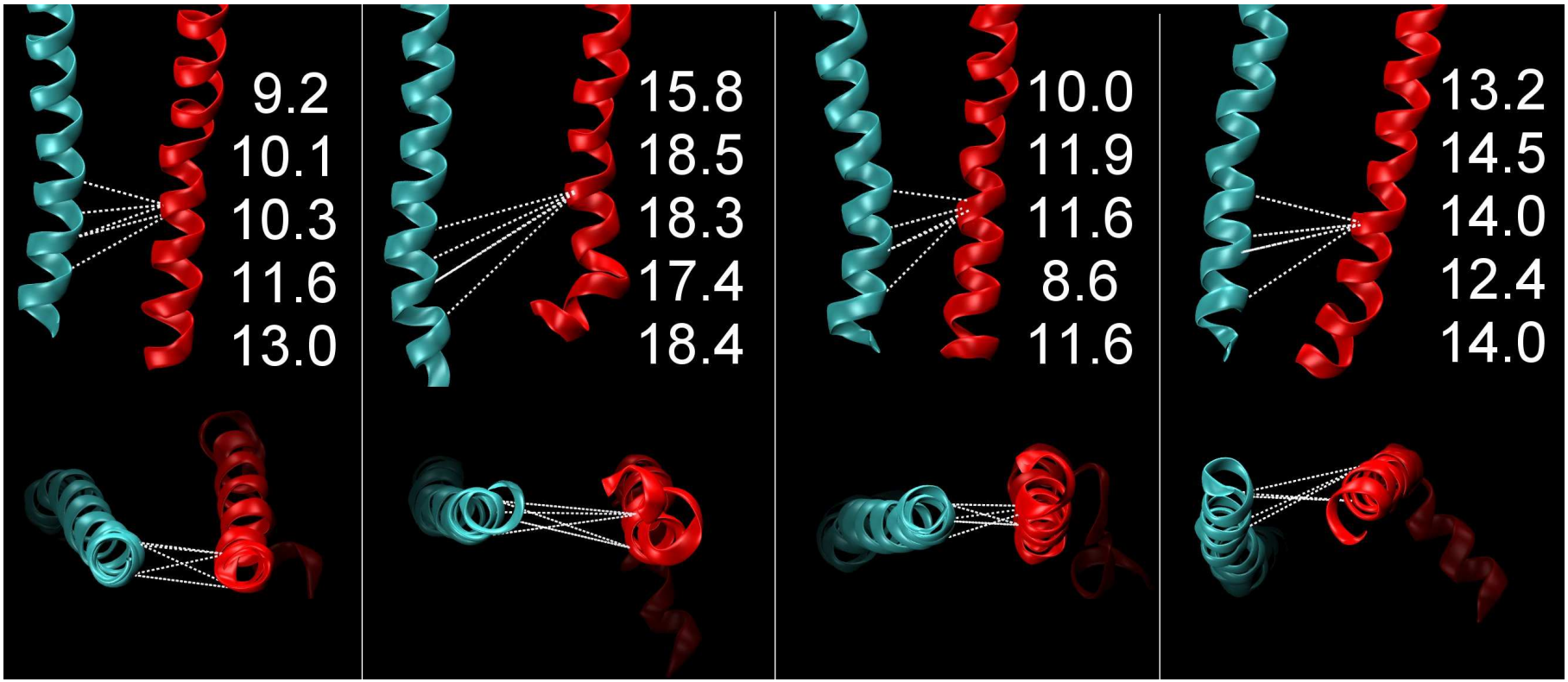

Supporting Figure S8. TM1 and TM11 Cross-linked Residue Orientations During Simulated Catalysis. The Figure shows the relative orientation of transmembrane helices 1 (light blue) and 11 (red) in the extracellular leaflet of the membrane. Residues 68 and 69 of TM 1 and residues 950, 953, 954 and 957 of TM 11, that were identified by Loo and Clarke and coworkers *(1)*in ATP hydrolysis dependent crosslinks are connected by white dashed lines. The lines from top to bottom in the figures connect Cα atoms of residues 68-950, 68-953, 68-954, 69-954 and 69-957, respectively. The four frames (left-to-right) correspond to "fully open inward", partially opened-inward",

“partially opened outward” and “fully opened outward” conformations. Calculated Cα to Cα distances in Å (same order as the connecting white lines) are given to the right of each frame. Images on the bottom of each panel show the same frame viewed from the extracellular space.

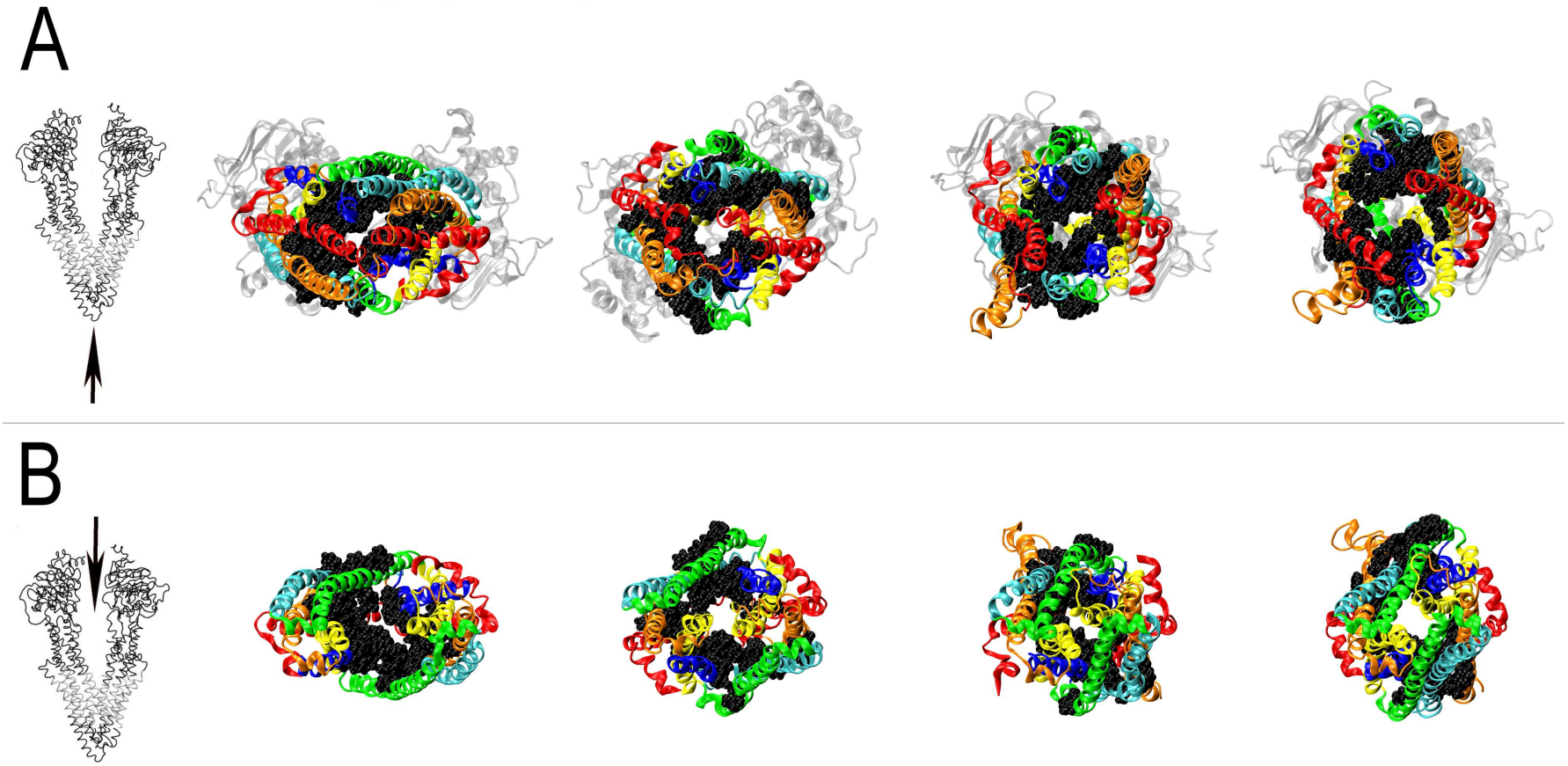
A
B

Supporting Figure S9. Views of the drug binding surfaces of Pgp during catalytic transitions. Images of the "fully opened inward", "partially opened inward", "partially opened outward" and "fully opened outward" are presented from the targeted MD docking trajectory from left to right. Amino acid residues observed to approach Pgp within 3.5Å are shown with van der Waal's surfaces in black. The protein backbone is shown in cartoon representation with the transmembrane helices shown with the following color code: Helices 1/7 red, 2/8 orange, 3/9 yellow, 4/10 green, 5/11 cyan and 6/12 are blue. **Panel A**: The top row of figures shows an extracellular view of Pgp with a viewpoint given by the tip of the arrow in the top-left image. Helix 1 (red) is to the left and helices 4 and 5 (green and cyan) are positioned at the top of all four frames of Panel A. **Panel B**: The bottom row of images views the drug binding domains from inside of the cytosolic portion of Pgp with a viewpoint given by the tip of the arrow in the bottom-left image (nucleotide binding domains have been removed for clarity). Helix 1 (red) is to the right and helices 4 and 5 (green and cyan) are positioned at the bottom of the four frames of Panel B.

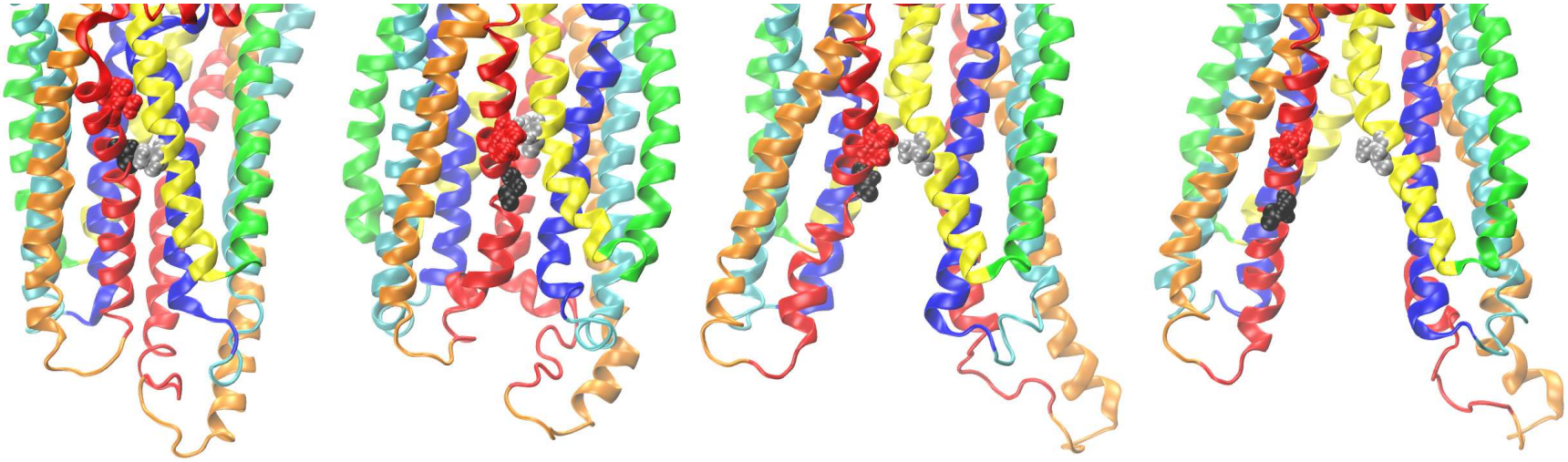

Supporting Figure S10. Possible exit gate in the drug binding domain of Pgp shown with color coded helices. The transmembrane helices of the drug binding domain of Pgp are shown in color coded cartoon representations. Helices 1/7 red, 2/8 orange, 3/9 yellow, 4/10 green, 5/11 cyan and 6/12 are blue. Alanine 841 is shown in the foreground on TM9 (yellow helix with gray space-filling representation), and V715 and G722 (both on the red TM7 helix shown in red and black space-filling representations, respectively). From left to right are shown the "fully opened inward", "partially opened inward", "partially opened outward" and "fully opened outward" conformations.

Table S1. List of P-glycoprotein Ligands Analyzed in this Work

Common name	Chemical name	Comments	Reference
Biricodar	1,7-dipyridin-3-ylheptan-4-yl (2S)-1-[2-oxo-2-(3,4,5-trimethoxyphenyl)acetyl]piperidine-2-carboxylate	Possible inhibitor of Pgp	(4)
CisZ-flupentixol	2-[4-[(3Z)-3-[2-(trifluoromethyl)thioxanthen-9-ylidene]propyl]piperazin-1-yl]ethanol	Dopamine antagonist; modulates Pgp activities	(5)
Cyclosporin A	(*E*)-14,17,26,32-tetrabutyl-5-ethyl-8-(1-hydroxy-2-methylhex-4-enyl) -1,3,9,12,15,18,20,23,27-nonamethyl-11,29-dipropyl-1,3,6,9,12,15,18,21,24,27,30-undecaazacyclodotriacontan-2,4,7,10,13,16,19,22,25,28,31-undecaone	Immune suppressant. Modulator of Pgp	(6)
Daunorubicin	(7S,9S)-9-acetyl-7-[(2R,4S,5S, 6S)-4-amino-5-hydroxy-6-methyloxan-2-yl]oxy-6,9, 11-trihydroxy-4-methoxy-8,10-dihydro-7H-tetracene-5,12-dione	An anthracine aminoglycoside from *Streptomyces sp.*; antineoplastic agent	(7)
Doxorubicin / Adriamycin	(7S,9S)-7-[(2R,4S,5S,6S)-4-amino-5-hydroxy-6-methyloxan-2-yl]oxy-6,9,11-trihydroxy-9-(2-hydroxyacetyl)-4-methoxy-8,10-dihydro-7H-tetracene-5,12-dione	An anthracine aminoglycoside from *Streptomyces sp.*; antineoplastic agent	(8)
Elacridar	N-[4-[2-(6,7-dimethoxy-3,4-dihydro-1H-isoquinolin-2-yl)ethyl]phenyl]-5-methoxy-9-oxo-10H-acridine-4-carboxamide	Pgp modulator	(9)
Hoechst33342	2-(4-ethoxyphenyl)-6-[6-(4-methylpiperazin-1-yl)-1H-benzimidazol-2-yl]-1H-benzimidazole	DNA topoisomerases inhibitor; Transport substrate for Pgp	(10)
Ivermectin	(2aE,4E,5'S,6S,6'R,7S,8E,11R,13R,15S,17aR,20R,20aR,20bS)-20,20b-dihydroxy-5',6,8,19-tetramethyl-6'-[(1S)-1-methylpropyl]-17-oxo-3',4',5',6,6',10,11,14,15,17,17a,20,20a,20b-tetradecahydro-2H,7H-spiro[11,15-methanofuro[4,3,2-pq][2,6]benzodioxacyclooctadecine-13,2'-pyran]-7-yl 2,6-dideoxy-4-O-(2,6-dideoxy-3-O-methyl-alpha-L-arabino-hexopyranosyl)-3-O-	Broad spectrum antiparasitic; collies with MDR1-deletion are over-sensitive	(11)

	methyl-alpha-L-arabino-hexopyranoside		
Lopinavir_AB1	(2S)-N-[(2S,4S,5S)-5-[[2-(2,6-dimethylphenoxy)acetyl]amino]-4-hydroxy-1,6-diphenylhexan-2-yl]-3-methyl-2-(2-oxo-1,3-diazinan-1-yl)butanamide	Anti-HIV protease inhibitor agent known to interact with Pgp	(12)
Paclitaxel	(2α,4α,5β,7β,10β,13α)-4,10-bis(acetyloxy)-13-{[(2*R*,3*S*)- 3-(benzoylamino)-2-hydroxy-3-phenylpropanoyl]oxy}- 1,7-dihydroxy-9-oxo-5,20-epoxytax-11-en-2-yl benzoate	An antineoplastic agent; stabilizes microtubules; Pgp substrate	(13)
QZ59S_RRR	(4R,5R,11R,12R,18R,19S)-4,11,18-TRIS(1-METHYLETHYL)-6,13,20-TRISULFUR-3,10,17,22,23,24-HEXAAZATETRACYCLO[17.2.1.1~5,8~.1~12,15~]TETRACOSA-1(21),7,14-TRIENE-2,9,16-TRIONE	RRR stereoisomer of sulfur substituted analog of selenium containing cyclic hexapeptide inhibitor of Pgp	(14)
QZ59S_SSS	(4R,5R,11R,12R,18R,19S)-4,11,18-TRIS(1-METHYLETHYL)-6,13,20-TRISULFUR-3,10,17,22,23,24-HEXAAZATETRACYCLO[17.2.1.1~5,8~.1~12,15~]TETRACOSA-1(21),7,14-TRIENE-2,9,16-TRIONE	SSS stereoisomer of sulfur substituted analog of selenium containing cyclic hexapeptide inhibitor of Pgp	(14)
Rhodamine123	[6-amino-9-(2-methoxycarbonylphenyl)xanthen-3-ylidene]azanium chloride	A Pgp transport substrate	(15)
Ritonavir	1,3-thiazol-5-ylmethyl N-[(2S,3S,5S)-3-hydroxy-5-[[(2S)-3-methyl-2-[[methyl-[(2-propan-2-yl-1,3-thiazol-4-yl)methyl]carbamoyl]amino]butanoyl]amino]-1,6-diphenylhexan-2-yl]carbamate	Anti-HIV protease inhibitor agent known to interact with Pgp	(12)
Saquinavir	(2S)-N-[(2S,3R)-4-[(3S,4aS,8aS)-3-(tert-butylcarbamoyl)-3,4,4a,5,6,7,8,8a-octahydro-1H-isoquinolin-2-yl]-3-hydroxy-1-phenylbutan-2-yl]-2-(quinoline-2-carbonylamino)butanediamide	Anti-HIV protease inhibitor agent known to interact with Pgp	(12)
Tamoxifen	2-[4-[(Z)-1,2-diphenylbut-1-enyl]phenoxy]-N,N-dimethylethanamine	Nonsteroidal antiestrogenic antineoplastic agent; Pgp substrate	(16)
Tariquidar	N-[2-[[4-[2-(6,7-dimethoxy-3,4-dihydro-1H-isoquinolin-2-yl)ethyl]phenyl]carbamoyl]-4,5-dimethoxyphenyl]quinoline-3-carboxamide	A Pgp modulator	(17)

Verapamil	(*RS*)-2-(3,4-dimethoxyphenyl)-5-{[2-(3,4-dimethoxyphenyl)ethyl]-(methyl)amino}-2-prop-2-ylpentanenitrile	Antihypertensive agent; Pgp modulator	(18)
Vinblastine	Dimethyl (2β,3β,4β,5α,12β,19α)- 15-[(5*S*,9*S*)- 5-ethyl- 5-hydroxy- 9-(methoxycarbonyl) - 1,4,5,6,7,8,9,10-octahydro- 2*H*- 3,7-methanoazacycloundecino[5,4-*b*]indol- 9-yl] - 3-hydroxy- 16-methoxy- 1-methyl-6,7-didehydroaspidospermidine- 3,4-dicarboxylate	A vinca alkaloid antineoplastic agent; a microtubule assembly inhibitor;	(8)
Zosuquidar	(2*R*)-1-{4-[(1a*R*,10b*S*)-1,1-difluoro-1,1a,6,10b-tetrahydrodibenzo[*a*,*e*]cyclopropa[*c*][7]annulen-6-yl}-3-(quinolin-5-yloxy)propan-2-ol	Possible inhibitor of Pgp	(19)
Valspodar	6-[(2S,4R,6E)-4-methyl-2-(methylamino)-3-oxo-6-octenoic acid]-Cyclosporin D	Possible inhibitor of Pgp; a non-immune suppressing cyclosporine derivative	(20)

Table S2. Listing of 3.5 Å close contacts between amino acids of human P-glycoprotein and docked ligands.

Any contact between protein and ligand that was less than or equal to 3.5 Å is listed in the table under its contacted amino acid number, the nonredundant molecular dynamics frame number from which the contact was detected, and the contacted Pgp residue type, number and helix.

summary_composite_3.5angstrom_close_contacts_data.rtf

SUPPORTING REFERENCES

1. Loo, T.W., Bartlett, M.C., and Clarke, D.M. (2005) Atp hydrolysis promotes interactions between the extracellular ends of transmembrane segments 1 and 11 of human multidrug resistance p-glycoprotein, *Biochemistry 44*, 10250-10258.

2. Loo, T.W., and Clarke, D.M. (1997) Drug-stimulated atpase activity of human p-glycoprotein requires movement between transmembrane segments 6 and 12, *J. Biol. Chem. 272*, 20986-20989.

3. Loo, T.W., and Clarke, D.M. (2001) Cross-linking of human multidrug resistance p-glycoprotein by the substrate, tris-(2-maleimidoethyl)amine, is altered by atp hydrolysis. evidence for rotation of a transmembrane helix, *J. Biol. Chem. 276*, 31800-31805.

4. Wang, S., Ryder, H., Pretswell, I., Depledge, P., Milton, J. et al. (2002) Studies on quinazolinones as dual inhibitors of pgp and mrp1 in multidrug resistance, *Bioorg. Med. Chem. Lett. 12*, 571-574.

5. Dey, S., Hafkemeyer, P., Pastan, I., and Gottesman, M.M. (1999) A single amino acid residue contributes to distinct mechanisms of inhibition of the human multidrug transporter by stereoisomers of the dopamine receptor antagonist flupentixol, *Biochemistry 38*, 6630-6639.

6. Nooter, K., Sonneveld, P., Oostrum, R., Herweijer, H., Hagenbeek, T. et al. (1990) Overexpression of the mdr1 gene in blast cells from patients with acute myelocytic leukemia is associated with decreased anthracycline accumulation that can be restored by cyclosporin-a, *Int. J. Cancer 45*, 263-268.

7. Shen, D.W., Fojo, A., Chin, J.E., Roninson, I.B., Richert, N. et al. (1986) Human multidrug-resistant cell lines: increased mdr1 expression can precede gene amplification, *Science 232*, 643-645.

8. Roninson, I.B., Chin, J.E., Choi, K.G., Gros, P., Housman, D.E. et al. (1986) Isolation of human mdr dna sequences amplified in multidrug-resistant kb carcinoma cells, *Proc. Natl. Acad. Sci. U.S.A. 83*, 4538-4542.

9. Wallstab, A., Koester, M., Böhme, M., and Keppler, D. (1999) Selective inhibition of mdr1 p-glycoprotein-mediated transport by the acridone carboxamide derivative gg918, *Br. J. Cancer 79*, 1053-1060.

10. Shapiro, A.B., and Ling, V. (1997) Positively cooperative sites for drug transport by p-glycoprotein with distinct drug specificities, *Eur. J. Biochem. 250*, 130-137.

11. Mealey, K.L., Bentjen, S.A., Gay, J.M., and Cantor, G.H. (2001) Ivermectin sensitivity in collies is associated with a deletion mutation of the mdr1 gene, *Pharmacogenetics 11*, 727-733.

12. Woodahl, E.L., Yang, Z., Bui, T., Shen, D.D., and Ho, R.J.Y. (2005) Mdr1 g1199a polymorphism alters permeability of hiv protease inhibitors across p-glycoprotein-expressing epithelial cells, *AIDS 19*, 1617-1625.

13. Greenberger, L.M., Lothstein, L., Williams, S.S., and Horwitz, S.B. (1988) Distinct p-glycoprotein precursors are overproduced in independently isolated drug-resistant cell lines, *Proc. Natl. Acad. Sci. U.S.A. 85*, 3762-3766.

14. Aller, S.G., Yu, J., Ward, A., Weng, Y., Chittaboina, S. et al. (2009) Structure of p-glycoprotein reveals a molecular basis for poly-specific drug binding, *Science 323*, 1718-1722.

15. Shapiro, A.B., and Ling, V. (1998) Stoichiometry of coupling of rhodamine 123 transport to atp hydrolysis by p-glycoprotein, *Eur. J. Biochem. 254*, 189-193.
16. Rao, U.S., Fine, R.L., and Scarborough, G.A. (1994) Antiestrogens and steroid hormones: substrates of the human p-glycoprotein, *Biochem. Pharmacol. 48*, 287-292.
17. Robey, R.W., Shukla, S., Finley, E.M., Oldham, R.K., Barnett, D. et al. (2008) Inhibition of p-glycoprotein (abcb1)- and multidrug resistance-associated protein 1 (abcc1)-mediated transport by the orally administered inhibitor, cbt-1((r)), *Biochem. Pharmacol. 75*, 1302-1312.
18. Cornwell, M.M., Pastan, I., and Gottesman, M.M. (1987) Certain calcium channel blockers bind specifically to multidrug-resistant human kb carcinoma membrane vesicles and inhibit drug binding to p-glycoprotein, *J. Biol. Chem. 262*, 2166-2170.
19. Lê, L.H., Moore, M.J., Siu, L.L., Oza, A.M., MacLean, M. et al. (2005) Phase i study of the multidrug resistance inhibitor zosuquidar administered in combination with vinorelbine in patients with advanced solid tumours, *Cancer Chemother. Pharmacol. 56*, 154-160.
20. te Boekhorst, P.A., van Kapel, J., Schoester, M., and Sonneveld, P. (1992) Reversal of typical multidrug resistance by cyclosporin and its non-immunosuppressive analogue sdz psc 833 in chinese hamster ovary cells expressing the mdr1 phenotype, *Cancer Chemother. Pharmacol. 30*, 238-242.